SAND2005-7876C

Structure of a Spatially-Developing Turbulent Lean Methane-Air Bunsen Flame

Ramanan Sankaran, Evatt R. Hawkes and Jacqueline H. Chen

Combustion Research Facility
Sandia National Laboratories, Livermore, CA 94551-0969

Tianfeng Lu and Chung K. Law

Department of Mechanical and Aerospace Engineering
Princeton University, Princeton, NJ 08540-5263

Corresponding author:
Dr. Ramanan Sankaran
Combustion Research Facility
Sandia National Labs
Livermore, CA 94551-0969.
Phone: (925) 294-1256
Fax: (925) 294-2595
email: rsankara@umich.edu

Word Count:

Text	4500 Words
Figures	(70 + 50 + 50 + 50 + 50 + 100 + 100) + (8×10) = 550mm
	550 × 2.2 = 1200 Words
Captions	200 Words
Total	5900 Words

Preferred colloquium topic area:
Turbulent Flames (Premixed Flames)

Keywords:
Turbulent combustion, premixed, DNS, thin reaction zone, flame structure

Submitted for presentation at the 31th Symposium (International) on Combustion
University of Heidelberg, Germany, August 6-11, 2006.

Abstract

Direct numerical simulation of a three-dimensional spatially-developing turbulent slot-burner Bunsen flame has been performed using detailed methane-air chemistry. The simulation is performed for three flow through times, long enough to achieve statistical stationarity. The turbulence parameters have been chosen such that the combustion occurs in the thin reaction zones regime of premixed combustion. The data is analyzed to study possible influences of turbulence on the structure of the preheat and reaction zones. The results show that the mean thickness of the turbulent flame is greater than the corresponding laminar flame. The effects of flow straining and flame front curvature on the mean flame thickness are quantified through conditional means of the thickness and by examining the balance equation for the evolution of the flame thickness. Finally, conditional mean reaction rate of key species compared to the laminar reaction rate profiles show that there is no significant perturbation of the heat release layer.

1 Introduction

In many practical applications for power generation, such as stationary gas turbines, there has been a strong interest in achieving lean premixed combustion due to the advantages of high thermal efficiency and low $\mathrm{NO_x}$ emissions. Lean flames tend to be thicker and propagate more slowly. Therefore, such devices have to operate at a higher turbulence intensity relative to the flame speed. Under these conditions, the flame structure may not be represented by a locally thin and one-dimensional flamelet. Recently, Peters [1] has provided a model for flame propagation in a regime where the turbulence is capable of influencing the preheat zone, but is incapable of penetrating the reaction zone. This regime is called the thin reaction zones (TRZ) regime. One of the challenges in this regime is to quantify the turbulent mixing in the preheat zone since it can directly influence the flame propagation speed. Furthermore, the integrity of the reaction layer needs to be verified for practical flames, such as methane-air flames, in which, contrary to the common theoretical assumption, the reaction zone is not an order of magnitude thinner than the preheat zone.

Direct numerical simulation (DNS) is an important tool for the study of turbulent combustion and provides valuable insight into the physics of flame-turbulence interaction. In the past, due to the limited computational resources, DNS of turbulent combustion was limited to simple configurations such as decaying turbulence in a periodic domain. Furthermore, complex chemistry simulations have been limited to two dimensions (2D) and three-dimensional (3D) simulations have been possible only with simple or tabulated chemistry. While these simplifications have been of great use in model development and validation in the past, they have lacked the realism of practical configurations. A spatially-developing flow configuration with at least one inflow is essential to represent laboratory-scale flames and to achieve statistical stationarity. While spatially developing flame simulations have been performed with simple or tabulated chemistry [2–4], recent advances in computer resources have made it possible to compute spatially-developing flows in 3D with detailed chemistry. Tanahashi *et al.* [5] and Bell *et al.* [6] have studied the propagation of hydrogen-air and methane-air flames, respectively, in 3D homogeneous turbulence at conditions

relevant to the TRZ regime.

Here, we have performed a fully-resolved DNS of a 3D spatially-developing lean methane-air Bunsen flame in the TRZ regime using detailed chemistry. The simulation has been advanced in time long enough to obtain statistical stationarity. The slot-burner Bunsen configuration is especially interesting due to the presence of mean shear in the flow and is similar in configuration to the burner used in experimental studies, such as by Filatyev *et al.* [7]. A new reduced chemical mechanism has been developed specifically for the present DNS of lean premixed methane-air flame at ambient pressure. The resulting mechanism has 13 transported species, 73 reactions and the quasi-steady state relations are solved analytically without need for costly non-linear iterations. The data obtained from the simulation is used to analyze the effect of turbulence on the preheat layer structure and flame thickness by obtaining the correlations of flame thickness with strain rate and curvature as a function of downstream position. The various contributions to a balance equation governing the evolution of the flame thickness are examined to better understand the cause of the thickening or thinning of the flame. Finally, the conditional mean reaction rate profiles are compared to unstrained and strained laminar flame solutions to determine the influence on the reaction layer.

2 Chemical Model

A reduced chemical mechanism for lean premixed methane-air flames was derived, specifically tailored to DNS needs such as minimum temporal stiffness. The reduction was accomplished through the sequential application of directed relation graph (DRG) [8], sensitivity analysis and computational singular perturbation (CSP) [9] over the GRI-1.2 detailed mechanism [10]. To assure minimal loss of kinetic information, the reduction was conducted by sampling a set of reaction states from two representative homogeneous applications: perfectly stirred reactor (PSR) that covers moderate to high temperature range where the radical pool already exists, and auto-ignition that covers the low to moderate temperature range where the radical pool needs to be built

up. The reaction states were sampled under atmospheric pressure, equivalence ratio (ϕ) from 0.6 to 0.9 for the intended lean combustion, and initial temperature from 1000 to 1800K for auto-ignition and 300K for PSR.

Figure 1 shows the dependence of the number of species in the skeletal mechanism as a function of the threshold value, ϵ, with the application of DRG, where ϵ indicates the maximum allowed relative error induced to the major species by species elimination [8]. It is seen that the species in the detailed mechanism can be divided into three groups: (i) Species with $\epsilon < 0.2$ are unimportant and can be safely removed. These are HCCO, $\mathrm{CH_2CO}$, HCCOH, $\mathrm{C_2H}$, $\mathrm{C_2H_2}$, $\mathrm{CH_3OH}$, $\mathrm{C_2H_3}$, C, $\mathrm{C_2H_4}$ and $\mathrm{C_2H_5}$. (ii) Species with $\epsilon > 0.5$ are important and have to be retained. (iii) Species with $0.2 < \epsilon < 0.5$ cannot be removed without further analysis of the sensitivity of global parameters. While such additional analysis is significantly more time consuming, the computational cost of DNS justified the effort. The global sensitivity of the flame speed to the elimination of each of the species was compared. As a result, $\mathrm{H_2O_2}$, $\mathrm{C_2H_6}$, $\mathrm{CH_3O}$, and CH were eliminated without loss of accuracy. The final skeletal mechanism contained 73 elementary reactions among 17 species, of which $\mathrm{CH_2}$, $\mathrm{CH_2(S)}$, HCO and $\mathrm{CH_2OH}$ were identified as quasi-steady state (QSS) species through CSP. The remaining 13 species were fully resolved, namely, $\mathrm{H_2}$, H, O, $\mathrm{O_2}$, OH, $\mathrm{H_2O}$, $\mathrm{HO_2}$, $\mathrm{CH_3}$, $\mathrm{CH_4}$, CO, $\mathrm{CO_2}$, $\mathrm{CH_2O}$ and $\mathrm{N_2}$. The QSS algebraic relations were solved analytically without the need for iterations, due to which complete convergence was obtained at a lower cost. Furthermore, the lack of iterations ensured good performance on vector computing platforms.

The resultant mechanism has been validated for flame speed and structure at the target mixture conditions and good agreement was obtained indicating that the crucial species and reaction pathways for high temperature chemistry are intact in the reduced mechanism. However, since the mechanism was reduced with lean methane-air flames in mind, it is not expected to be valid for rich conditions or ignition problems.

3 Computational Approach

A planar-jet turbulent Bunsen flame configuration was used. Preheated methane-air mixture at 800K and ϕ = 0.7 flows through a rectangular slot. The reactant jet is surrounded by a hot coflow whose composition and temperature are those of the complete combustion products of the main jet, similar to the pilot flame surrounding slot burners commonly used in experiments [7]. At these conditions, the unstrained laminar flame properties computed using PREMIX [11] are: (i) flame speed, $S_{\rm L}$ = 1.8 m/s (ii) thermal thickness based on maximum temperature gradient, $\delta_{\rm L}$=0.3mm (iii) full width at half maximum (FWHM) of heat release rate, $\delta_{\rm H}$ = 0.14mm, and (iv) flame time scale, $\tau_{\rm f}$=$\delta_{\rm L}/S_{\rm L}$=0.17ms. While the preheated inflow condition has been chosen for numerical reasons (the cost of computation is inversely proportional to the Mach number at inflow), many practical devices such as internal combustion engines, gas turbines and recirculating furnaces operate at highly preheated conditions. Also, the preheat is low enough that flameless combustion [12] does not occur. One consequence of preheating is that the reaction zone is broadened at 800K ($\delta_{\rm L}/\delta_{\rm H}$=2) compared to 300K ($\delta_{\rm L}/\delta_{\rm H}$=3).

The domain sizes in the streamwise (x), crosswise (y) and spanwise (z) directions, in terms of the slot width (h = 1.2mm), are $L_x \times L_y \times L_z = 12h \times 12h \times 3h$. A uniform grid spacing of 20μm was used in the x and z directions, while an algebraically stretched mesh in the y direction was obtained from $y(s) = f(s) \times s$, where s is the equi-spaced computational grid and $0 \leq s \leq 1$. The stretching function is given by,

$$f(s) = \beta s + \frac{1}{2}\left(1 + \tanh\frac{s - s^*}{\sigma}\right)\left(e^{ks} - \beta s\right), \tag{1}$$

where $k = \ln(\beta s^*)/(s^* - 1)$. The resultant mesh was mirrored across the jet centerline ($y = s = 0$) to get a symmetric mesh. The form of the stretching function along with the choice of constants, $\beta = 0.55$, $s^* = 0.75$ and $\sigma = 1/16$, yields a mesh that has a uniform spacing of 20μm in a 6mm wide region in the center and stretches outward with a rate of increase in grid spacing ($\Delta_{i+1}/\Delta_i - 1$) no more than 2%. While the uniform grid spacing at the center of the jet ensures numerical fidelity

and flexibility in post-processing, the boundaries are pushed farther away to reduce their influence on the flame. The resultant mesh size was $N_x \times N_y \times N_z = 720 \times 400 \times 180$.

The flame was anchored at the inflow plane by specifying the species mass fractions and temperature from an unstrained laminar flame solution using a progress variable lookup. A hyperbolic tangent function was used to obtain a smooth variation of progress variable between the unburned and burned conditions. The velocity field at the inflow boundary was obtained by performing a separate temporally-developing simulation of a streamwise periodic flow. This secondary simulation was performed for a short period of time to allow sufficient development of the flow field and the resultant field was then frozen (in time) to obtain the inflow conditions for the main simulation using Taylor's hypothesis. The mean and fluctuating velocity profiles at the inlet, $\tilde{U}$ and u', where $\tilde{}$ denotes Favre averaging, are shown in Fig. 2. Based on the centerline inlet velocity, a flow through time is defined as $\tau_{\mathrm{U}} = 0.24$ms. Due to the presence of mean shear in the configuration, the turbulence scales continue to evolve downstream, which is discussed in a later section. The boundary conditions are periodic in z, non-reflecting inflow and outflow in x, and non-reflecting outflow [13] in y.

The simulations were performed using the DNS code S3D, which solves the fully compressible Navier Stokes, species and energy equations with a fourth-order Runge-Kutta method for time integration and an eighth-order explicit spatial differencing scheme [14, 15]. A tenth-order filter was used periodically to damp any spurious high-wave number oscillations. The mixture specific heat is determined locally as a function of the mixture composition and temperature. The molecular viscosity is also temperature dependent and the species Lewis numbers are assumed to be constant. The solution was advanced at a constant 2ns time-step for three flow through times, of which the first was neglected due to initial transients when collecting statistics. Data from 61 equally spaced time instants requiring approximately 0.5TB in disk space was analyzed. In the following section, the statistical structure of the flame is presented in terms of Favre averages. Averaging is performed in the homogenous direction (z), and time. Symmetry across the centerline is exploited.

4 Results and Discussion

4.1 General description and flow characteristics

First, we present the characteristics of the instantanenous flame front identified using a progress variable, c. While c is usually defined based on the deficient reactant, in this case the fuel, such a definition here will omit a significant portion of the oxidation layer, since the heat release is only 66% complete where CH_4 is completely consumed. Therefore, c is obtained using O_2 mass fraction. The flame surface is defined as $c = 0.65$, which corresponds to the location of maximum heat release in an unstrained laminar flame. Figure 2 shows the flame surface after one flow through time. The flame is initially planar near the inlet and shows considerable development with downstream distance. It is well wrinkled and the scale of wrinkling progressively gets larger. The shape of the flame is mostly convex towards the products and forms cusps towards the reactants, contrary to Huygens propagation. Evidently, turbulent straining has a stronger influence on the flame topology than self-propagation. Further downstream, the surface shows large scale roll-ups due to the presence of mean shear and mixing layer instability, leading to pinch off at the tip. The average turbulent flame brush, as seen from the contour plot of $\tilde{c}$, grows with x. The contour plot also shows the location of the shear layer, defined as the location of maximum velocity gradient ($d\tilde{U}/dy$), along with the average flame location. It is seen that, at x=0, the flame resides outside of the shear layer and progressively moves towards the inside as increasing amounts of fuel are consumed. However, for a significant fraction of the domain, the flame resides in the core of the turbulent jet.

Since there is significant axial development of the flame, the results are presented at selected x locations denoted by their distance from the inflow plane as a fraction of L_x, namely, '0', '1/4', '1/2' and '3/4'. Figure 3 shows the change in profiles of velocity fluctuation, u' and turbulent length scale, l_t, as the jet develops. Here, l_t is estimated using the average turbulent kinetic energy dissipation rate, $\tilde{\epsilon}$, as $l_t = u'^3/\tilde{\epsilon}$. It is seen that u' decays rapidly close to the inlet but does not vary significantly past the initial 1/4th of the domain. On the other hand, l_t continues to increase

with downstream distance. As a whole, the flame can be characterized by, approximately, $u'/S_{\rm L}$=3 and $l_{\rm t}/\delta_{\rm L}$=1, which places it in the TRZ regime of combustion close to the boundary with the corrugated flamelets regime. Although it is desirable to perform the study at a higher turbulence intensity and larger length scale, the turbulence injection procedure used here can lead to instability at the inlet unless the jet size is increased proportionately, thereby restricting the feasible turbulence level. Simulations at a higher turbulence level along with improvements to the inflow boundary condition are a topic of ongoing investigation.

4.2 Effect on flame thickness

In this section we study the effect of turbulent stirring on the flame thickness. It has been proposed [1] that in the TRZ regime, the turbulent eddies can penetrate the preheat zone and increase the mixing process, leading to a thicker flame. However, the results of experimental studies in this regime are contradictory, with some reports of thicker flames [16, 17] and others of thinner flames [18, 19]. See Ref. [20] for a detailed discussion of the contrasting experimental results on this topic. Computational studies have not yet yielded a definitive conclusion on the flame thickness issue either. Although some computational studies [21, 22] have found that, on average, the flame gets thinner, the results are not conclusive due to the lack of realism in 2D turbulence in Ref. [21] and statistical stationarity in Ref. [22]. Here, we analyze the current simulation results to determine if, on average, the flame thickness increases or decreases relative to a laminar flame.

The magnitude of the progress variable gradient, $|\nabla c|$, is averaged over intervals of c and compared with the unstrained laminar flame profile in Fig. 4. Also the distribution of $|\nabla c|$ at the location of steepest gradient, $c = 0.5$, is shown on the right for reference. The reciprocal of $|\nabla c|$ yields a flame thickness analogous to the definition used for $\delta_{\rm L}$. The results show that $|\nabla c|$ is consistently lower than the laminar value and decreases with increasing x. At the '1/4'th location, a portion of the preheat layer closest to the fresh mixture has a mean gradient equal to the laminar flame thickness. This can be attributed to the finite response time of the flame such that it does not instantaneously respond to the imposed fluctuations [23] and remains close to the laminar flame

profile. However, at all other downstream locations, the average gradients in the preheat zone are clearly lower, pointing to a thickening of the flame. No significant deviation is seen for values of c close to unity, which corresponds to the oxidation layer. While this indicates that there is no disruption of the oxidation layer by turbulence, this aspect is discussed in a later section in greater detail through an analysis of the reaction rates of keys species.

Fig. 4 shows that, although there is some probability (27%, 20% and 8% at locations '1/4', '1/2' and '3/4' respectively) of encountering a thinner flame, on average the flame thickness increases. This is in agreement with some, although not unanimous, experimental results [16, 17]. At this stage, it is instructive to study the effect of strain rate since flow straining is one of the possible causes identified by experiments [18] that observed flame thinning. It has been established that due to preferential alignment of scalar gradient with flow strain, the mean tangential strain rate on a scalar iso-surface is positive [24]. Therefore, it seems counter-intuitive that a flame with positive mean strain rate would become thicker rather than thinner. Therefore, the conditional average of $|\nabla c|$ on the $c = 0.5$ iso-surface is compared with the laminar strained flame solution up to the extinction strain rate, obtained using OPPDIF [25]. The mean flame thickness shows a strong correlation with the tangential strain rate as evident from Fig. 5. However, a higher sensitivity to strain rate relative to the laminar solution and a consistently thicker flame are observed, which can be attributed to a stronger influence of the small scale eddy mixing compared to large scale flow straining. Figure 5 also shows a significant probability for compressive (negative) strain (40%, 35% and 25% at locations '1/4', '1/2' and '3/4', respectively) which leads to significant thickening of the flame in those regions. Since compressive strain tends to be associated with highly curved flame elements, the effect of flame front curvature is studied next.

4.3 Curvature and flame thickness

Curvature of an iso-surface $c = c^*$ is given by $(\nabla \cdot n)_{c=c^*}$, where n=$-\nabla c/|\nabla c|$ is the unit vector normal to the surface and pointing towards reactants. By definition, a positive curvature denotes a surface convex to the reactants. Fig. 6 shows the mean thickness conditional on curvature, on the

$c = 0.5$ iso-surface at the chosen streamwise locations along with the distribution of curvature at these locations. It is seen that the distribution of curvatures is not symmetric about zero and has a longer tail for positive curvatures. This confirms the observation made earlier that turbulence dominates over laminar propagation to form sharp positive cusps, contrary to Huygens propagation. A negative correlation between $|\nabla c|$ and curvature is seen, in agreement with the results in Ref. [2]. The results show that the flame becomes increasingly thicker with curvature, and more so at positively curved convex regions in comparison to the negatively curved regions. Furthermore, an asymmetry in the dependence of $|\nabla c|$ on curvature is observed, whereby the lowest average flame thickness occurs at a slightly negative curvature, approximately equal to $1/\delta_{\mathrm{L}}$.

To further understand the role of curvature on thickening of the flame, a balance equation for the material derivative of $|\nabla c|$ on the progress variable iso-surface is written as [26],

$$\frac{D}{Dt}|\nabla c| = -\left(a_{\mathrm{n}} + \frac{\partial S_{\mathrm{d}}}{\partial n}\right)|\nabla c| \tag{2}$$

where, the normal strain, a_{n}, is given in terms of the dilatation (a_{d}) and the tangential strain rate (a_{t}) as $a_{\mathrm{n}} = a_{\mathrm{d}} - a_{\mathrm{t}}$. Furthermore, the propagation speed S_{d} is decomposed into its reaction, normal diffusion and curvature components as $S_{\mathrm{d}} = S_{\mathrm{d,r}} + S_{\mathrm{d,n}} + S_{\mathrm{d,c}}$ [27]. From Eq. 2 it is seen that the terms on the RHS can act as a source or sink for $|\nabla c|$, thereby leading to thinner or thicker flames, respectively. A budget of the different terms conditional on curvature at c=0.5 is shown in Fig. 7 leading to the following observations. First, tangential strain rate is found to be negatively correlated with curvature and therefore highly curved regions have lower values of a_t and vice versa. Furthermore, it is seen that at large positive values of curvature, the strain rate can become compressive. Such compressive strains are not observed statistically at large negative values of curvature due to the dearth of sharp cusps in those parts of the flame. Positive values of the tangential strain rate act as a source of $|\nabla c|$ and hence cause a thinning of the flame. Second, as the tangential strain rate decays in the downstream direction, the sum of the reaction and normal diffusion components, otherwise known as kinematic restoration term [1], $\partial S_{\mathrm{d,r+n}}/\partial n$, also decays to restore the balance. However, by the '3/4'th position, the kinematic restoration is significantly

reduced such that the strain rate is mainly counteracted by dilatation. Third, for small curvatures, $-2 < |\nabla \cdot n|\delta_{\mathrm{L}} < 2$, $\partial S_{\mathrm{d,c}}/\partial n$ is relatively small in comparison to the other terms and the tangential strain is primarily counteracted by dilatation and kinematic restoration. However, for large values of curvature, the curvature term is significant and acts as a sink for $|\nabla c|$ leading to thicker flames. Thus, the source of the variation in flame thickness can be explained using Eq. 2. Further insight can be obtained by tracking the history of iso-surface elements as they propagate and convect across the domain [28].

4.4 Reaction zone structure

To study the effect of turbulence on the structure of the reaction zone, the conditional means of $\mathrm{CH_4}$, CO and OH production rates are determined and compared with the laminar reaction rate profiles in Fig. 8. The laminar solution is obtained for both an unstrained flame and a strained flame at $a_{\mathrm{t}}\tau_{\mathrm{f}}$ = 1.5, which approximately equals the mean tangential strain rate in the flame (see Fig. 5). The results show that the two laminar flame solutions effectively encompass the average reaction rates. At the '1/4'th location the mean profiles agree well with the stretched flame solution. At other downstream locations, the reaction rates are initially close to the stretched flame solution for small values of c, but move towards the unstrained flame solution as c increases. Overall, it seems that closures based on conditional laminar reaction rates and a PDF of the progress variable [29] will perform well in predicting the turbulent burning rate. The results confirm the hypothesis [1] that, in the TRZ regime, the turbulent eddies do not significantly disrupt the reaction zone. Since the reaction zone here is not really thin ($\delta_{\mathrm{L}}/\delta_{\mathrm{H}} \approx 2$), the lack of significant influence on the reaction layer is attributed to the dissipation of turbulence resulting from heat release.

5 Conclusions

A spatially-developing 3D Bunsen flame was simulated using a computationally accurate and efficient detailed $\mathrm{CH_4}$-air chemical mechanism derived specifically for this purpose. The results show thickening of the preheat zone due to the action of turbulent eddies, in spite of the presence of a

mean positive strain rate. The correlations of flame thickness with strain rate and curvature were obtained. A balance equation for the iso-surface substantial derivative of the progress variable gradient was used to study the contribution of various terms that influence the flame thickness. It was found that, at small curvatures, tangential strain rate is counteracted by dilatation and the normal gradient of kinematic restoration, while at large curvatures the normal gradient of curvature component of propagation is a significant source of flame thickening. Finally, the conditional mean reaction rates of key species were compared with unstrained and strained laminar flame solutions. The good agreement with laminar solutions points towards reaction rate closure based on conditional laminar reaction rates in this regime.

Acknowledgements

The work at SNL was supported by the Division of Chemical Sciences, Geosciences and Biosciences, the Office of Basic Energy Sciences (BES), the U.S. Department of Energy (DOE) and also by the U.S. DOE, BES, SciDAC Computational Chemistry program. The work at Princeton was supported by the Air Force Office of Scientific Research under the technical monitoring of Dr. Julian M. Tishkoff. This research used resources of the National Center for Computational Sciences (NCCS) at Oak Ridge National Laboratory (ORNL), which is supported by the Office of Science of the U.S. Department of Energy under Contract No. DE-AC05-00OR22725. We are grateful to Mark R. Fahey of NCCS/ORNL for his computing support.

References

[1] N. Peters, *J. Fluid Mec.* 384 (1999) 107–132.

[2] N. Chakraborty, R. S. Cant, *Physics of Fluids* 17 (2005) 065108.

[3] T. M. Alshaalan, C. J. Rutland, *Combust. Sci. Technol.* 174 (2002) 793–799.

[4] L. Vervisch, R. Hauguel, P. Domingo, M. Rullaud, *Journal of Turbulence* 5 (2004) 004.

[5] M. Tanahashi, Y. Nada, Y. Ito, T. Miyauchi, *Proc. Combust. Inst.* 29 (2002) 2041–2049.

[6] J. B. Bell, M. S. Day, J. F. Grcar, *Proc. Combust. Inst.* 29 (2002) 1987–1993.

[7] S. A. Filatyev, J. F. Driscoll, C. D. Carter, J. M. Donbar, *Combust. Flame* 141 (2005) 1–21.

[8] T. Lu, C. K. Law, *Proc. Combust. Inst.* 30 (2005) 1333–1341.

[9] T. Lu, Y. Ju, C. K. Law, *Combust. Flame* 126 (2001) 1445–1455.

[10] M. Frenklach, H. Wang, M. Goldenberg, G. P. Smith, D. M. Golden, C. T. Bowman, R. K. Hanson, W. C. Gardiner, V. Lissianski, *GRI-Mech: An Optimized Detailed Chemical Reaction Mechanism for Methane Combustion*, Tech. Rep. GRI-95/0058, Gas Research Institute (1995).

[11] R. J. Kee, J. F. Grcar, M. D. Smooke, J. A. Miller, *PREMIX: A Fortran Program for Modeling Steady Laminar One-Dimensional Premixed Flames*, Tech. Rep. SAND85-8240, Sandia National Laboratories (1985).

[12] T. Plessing, N. Peters, J. G. Wunning, *Proc. Combust. Inst.* 27 (1998) 3197–3204.

[13] T. J. Poinsot, S. K. Lele, *J. Comp. Phys.* 101 (1992) 104–129.

[14] C. A. Kennedy, M. H. Carpenter, *Appl. Num. Math.* 14 (4) (1994) 367–458.

[15] C. A. Kennedy, M. H. Carpenter, R. M. Lewis, *Appl. Num. Math.* 35 (3) (2000) 177–264.

[16] M. S. Mansour, N. Peters, Y. C. Chen, *Proc. Combust. Inst.* 27 (1998) 767–773.

[17] Y. C. Chen, M. S. Mansour, *Proc. Combust. Inst.* 27 (1998) 811–818.

[18] F. Dinkelacker, A. Soika, D. Most, D. Hofmann, A. Leipertz, W. Polifke, K. Dobbeling, *Proc. Combust. Inst.* 27 (1998) 857–865.

[19] A. Soika, F. Dinkelacker, A. Leipertz, *Proc. Combust. Inst.* 27 (1998) 785–792.

[20] F. Dinkelacker, in: *Proceedings of the European Combustion Meeting*, 2003, paper no. 158.

[21] E. R. Hawkes, J. H. Chen, in: *Proceedings of the 2003 Winter Meeting of the Western States Section of the Combustion Institute*, 2003, paper no. 03F-68.

[22] D. Thevenin, *Proc. Combust. Inst.* 30 (2005) 629–637.

[23] H. G. Im, J. H. Chen, *Proc. Combust. Inst.* 28 (2000) 1833–1840.

[24] W. T. Ashurst, A. R. Kerstein, R. M. Kerr, C. H. Gibson, *Physics of Fluids* 30 (8) (1987) 2343–2353.

[25] A. E. Lutz, R. J. Kee, J. F. Grcar, F. M. Rupley, *OPPDIF: A Fortran Program for Computing Opposed-Flow Diffusion Flames*, Tech. Rep. SAND96-8243, Sandia National Laboratories (1997).

[26] S. B. Pope, *Int. J. Eng. Sci.* 26 (1988) 445–469.

[27] T. Echekki, J. H. Chen, *Combust. Flame* 118 (1999) 308–311.

[28] P. Sripakagorn, G. Kosaly, J. J. Riley, *Combust. Flame* 136 (2004) 351–363.

[29] B. Fiorina, O. Gicquel, L. Vervisch, S. Carpentier, N. Darabiha, *Proc. Combust. Inst.* 30 (2004) 867–874.

List of Figures

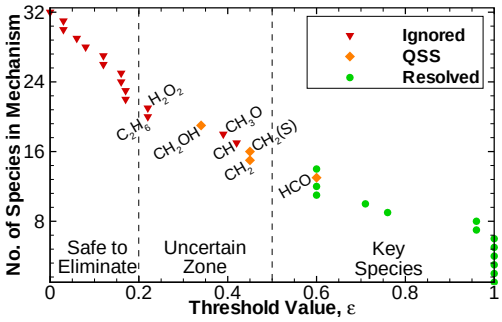

Figure 1: Number of species in skeletal mechanism as a function of the threshold value ϵ in skeletal reduction with directed relation graph.

Color in PDF only

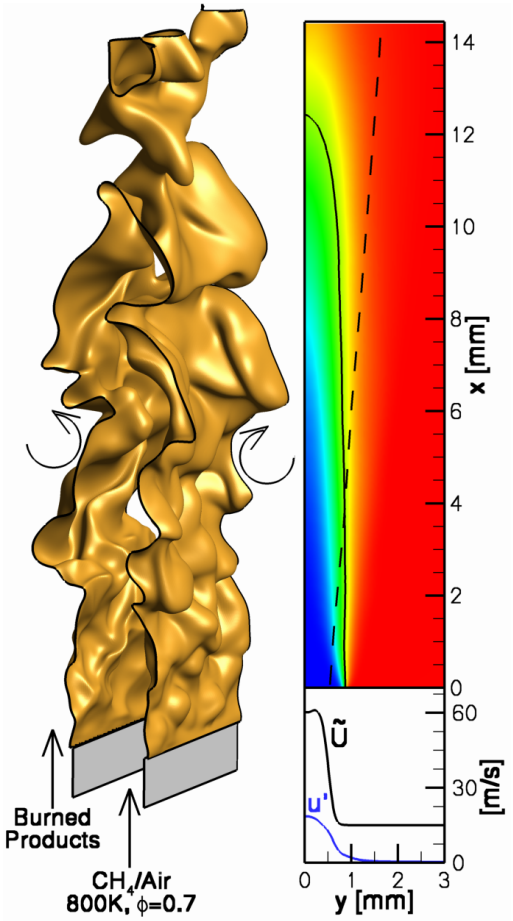

Figure 2: Shown on the left is the instantaneous iso-contour of c=0.65 at t=1τ_{U}. On the top right, the contour plot of $\tilde{c}$ shows the average flame brush location. The color scale varies from blue (0) to red (1). Also shown on the contour plot are the iso-contour of $\tilde{c} = 0.65$ (solid line) and the location of the shear layer (dashed line). The bottom right shows the mean and fluctuating velocity profiles at the inlet.

Color in Print and PDF

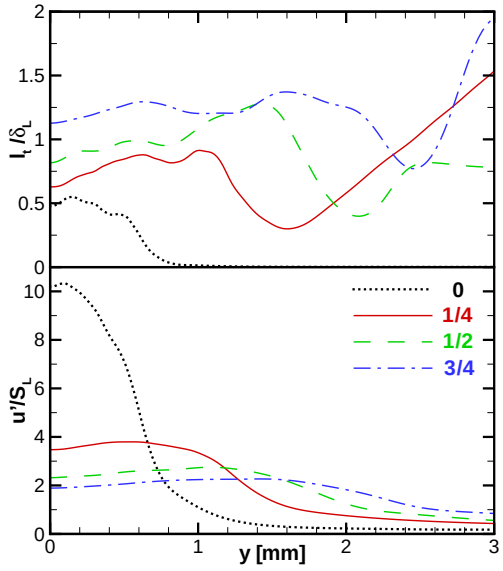

Figure 3: Profiles of u'/S_{L} and l_t/δ_{L} at different streamwise locations, denoted by their distance from the inflow plane as a fraction of L_x.

Color in PDF only

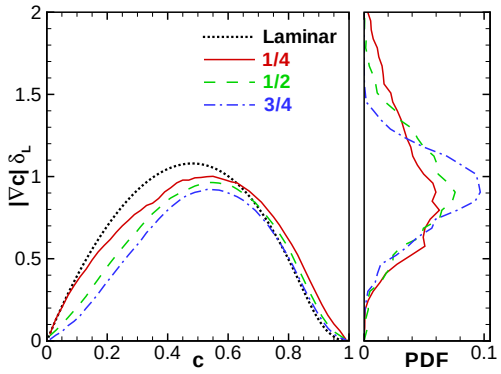

Figure 4: Conditional means of $|\nabla c|$ compared to the unstrained laminar flame profile. Shown on the right is the PDF of $|\nabla c|$ at c=0.5.

Color in PDF only

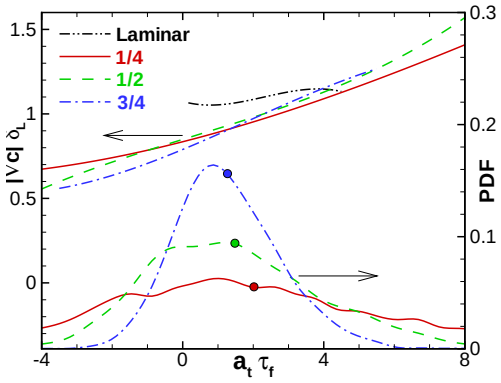

Figure 5: Average $|\nabla c|$ conditional on a_{t} and PDF of a_{t} on the c=0.5 iso-surface compared to the strained laminar flame. Filled circles mark the mean a_{t} at the respective x-locations.

Color in PDF only

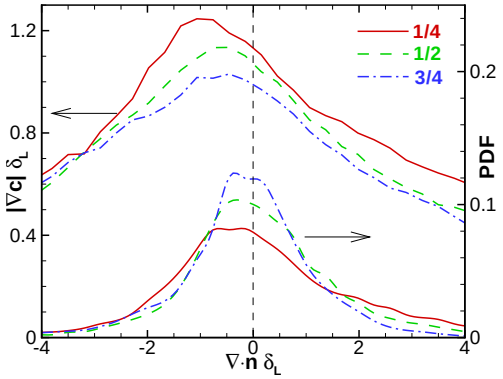

Figure 6: Average $|\nabla c|$ conditional on curvature and PDF of curvature on the c=0.5 iso-surface compared to the strained laminar flame.

Color in PDF only

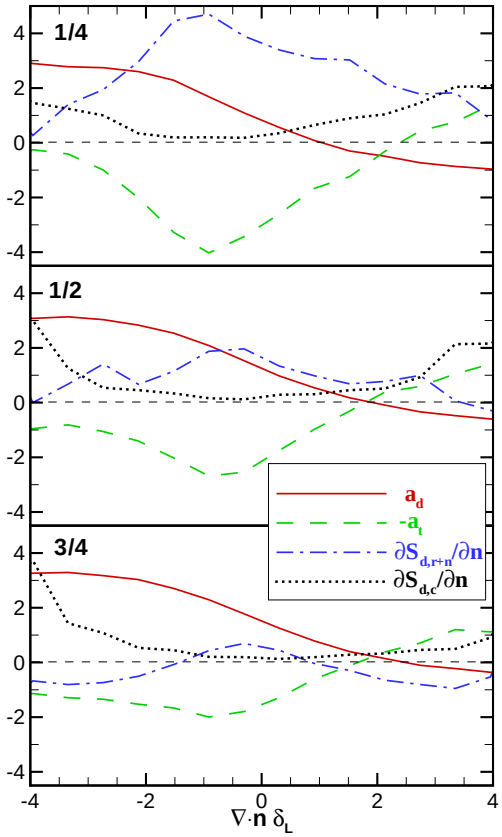

Figure 7: Budget of the source terms in Eq. 2 as a function of curvature at the three chosen streamwise locations. The terms are non-dimensionalized using τ_f.

Color in PDF only

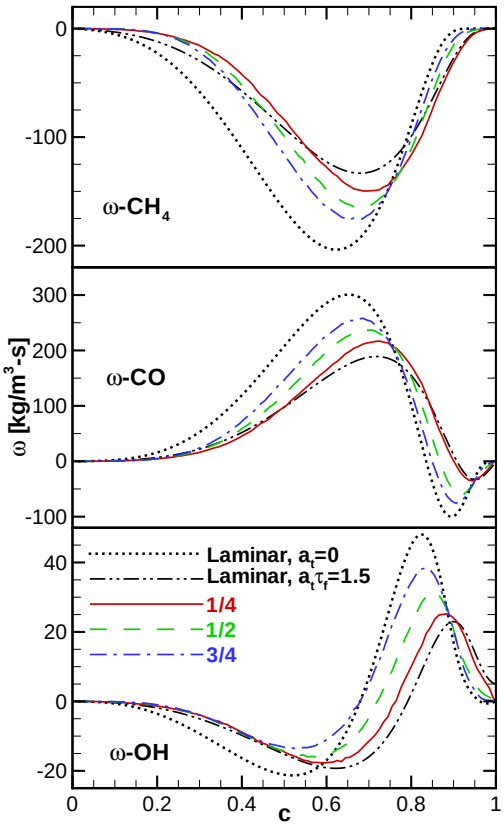

Figure 8: Average reaction rates conditional on the progress variable (c) compared to laminar flame reaction rate profile.

Color in PDF only